Testing and Analyzing of Distance Protection of a Realistic Offshore Wind Farm Transmission System

de Korte, Kasper; van Dijk, Gerwin; Yelgin, Yilmaz ; Chavez, Jose; Popov, Marjan

Publication date
2022

Document Version
Final published version

Published in
Cigre Session 2022

10552 Session 2022
B5 – Protection and Automation
PS1 / Addressing protection related challenges in network with low-inertia and low fault-current levels

Testing and Analyzing of Distance Protection of a Realistic Offshore Wind Farm Transmission System

Kasper DE KORTE[1*], Gerwin VAN DIJK[1], Yilmaz YELGIN[2], Jose CHAVEZ[3] & Marjan POPOV[3]
1. Siemens Nederland N.V., The Netherlands,
Kasper.deKorte@siemens.com, Gerwin.van.Dijk@siemens.com
2. Siemens A.G., Germany,
Yilmaz.Yelgin@siemens.com
3. Delft University of Technology, The Netherlands,
M.Popov@tudelft.nl, J.J.ChavezMuro@tudelft.nl

SUMMARY

Protection schemes are implemented to address dependability and security during a fault in the transmission system. Overall, the distance protection function plays an important role as it is commonly employed as primary or backup protection because of its speed and accuracy. The transmission system is in charge to interconnect offshore wind farms with hundreds of megawatts to onshore grids.. Normally, a distance protection relay responds correctly to the majority of faults in a wind farm electrical grid. However, there are certain cases when the protection relay may fail to operate correctly.

In order to examine the performance of the protection relay, this paper analyses test results using software simulation and partial testing. Partial testing is a method where simulated signals, at chosen locations, are extracted from the simulated grid, synthesized to real voltages and currents, and connected to the protection relay. The model used in this work represents an actual wind farm grid and is suitable for electromagnetic transient simulations. Wind turbine models based on a doubly-fed induction machine with rotor connected converters are used in the simulation. The fault variables are symmetrical and asymmetrical faults, fault locations, faulty phases, arc resistance, grid strength, and infeed power. The total of cases result in 170 fault scenarios that are observed and analysed. The secondary signals, voltages and currents from the instrument transformers are extracted from the simulation and synthesized with a signal generator. The protection relay is connected to the signal generator and fed by test signals.

Each scenario is carried out for three locations on the grid by utilizing two different protection functions; the classic distance protection method and the distance protection method with reactance method (RMD).

The tests have shown that the dynamic behavior of a wind farm electrical grid can compromise the classic distance protection method. Moreover, it has been seen that the distance protection method based on the RMD method provide higher performance in these scenarios.

Therefore, the findings from this study can be used to assemble a more reliable protection scheme where multiple protection functions are combined.

Similar studies investigate a theoretical grid. This study is a valuable addition to earlier research since an existing system is investigated for wind farms in the largest category. Furthermore, this paper compares two distance protection methods, the classic method and RMD method, whereas other studies only analyze one distance protection method. A deliberate protection strategy can be formed based on the observations described in this article.

KEYWORDS

Distance protection relay, wind farm, transmission grid, testing, simulation.

INTRODUCTION

The installed capacity of renewable energy sources increases faster than other energy sources. Governments steer to more renewable energy sources (RES) to reduce the CO2 emissions and dependencies of fossil fuels [1]. Wind and solar generator properties are different from synchronous generators with a large inertia. One of these properties is that wind and solar energy are often distributed generation (DG) instead of centralized generation. An increase in the proportion of wind and solar energy change the behavior of the grid. Fault protection of the grid must adapt to this change. The literature has been reported and analyzed in some cases the distance protection function failures near DG [2] [3].

This work aims to identify potential problems with the protection of a grid with high penetration of RES and find its cause. In order to have a realistic case, a protection scheme similar to a real offshore wind power plant is studied. An offshore grid connects the wind turbines to the on-shore transmission grid. Although the protection scheme of this transmission system uses multiple types of protection methods, in this study only the distance protection of the offshore transmission grid is considered.

Based on the results of simulation and tests, unexpected behavior could be detected, and mitigating measures can be proposed. Similar studies have been carried out on this topic and earlier studies have shown that there is a difference in manufacturer of protection devices if it comes to certainty of tripping [4]. Therefore, new insights into the protection scheme can help further studies to improve the protection scheme. This can eventually result in an optimization of the grid protection and therefore decrease the unavailability of the electricity grid.

The main purpose of this study is to verify if the distance protection with the classic method, and distance protection with the reactance method (RMD), respond correctly to a wind farm electrical grid. This includes simulating the grid using an electromagnetic transient (EMT) simulation, developing a test setup, carrying out the test, and identifying unexpected results. Included in this study is to find the cause of an unexpected result.

A detailed model of the grid is made in power engineering simulation software. Voltages and currents are extracted and synthesized to feed real protection devices. The behavior of the protection relay is analyzed. Unexpected behavior is studied. The result of the analysis can point out parts of the protection scheme that needs to be improved or confirm that it works as desired.

1 Impedance calculation

Two distance protection methods are studied. The classic distance protection and the RMD method. Both methods use the measured voltages and currents to calculate the impedance each with its own equation. If the loop impedance is calculated in a preset quadrilateral characteristic the protection relay gives a pickup signal.
With both distance protection methods, the line-to-line fault impedance is calculated by:

$$\underline{Z}_{L_A-L_B} = \frac{\underline{U}_{L_{A-G}} - \underline{U}_{L_{B-G}} - R_F\underline{I}_F}{\underline{I}_{L_A} - \underline{I}_{L_B}} \quad \textbf{(1)}$$

Where $\underline{U}_{L_{A-G}}$, $\underline{U}_{L_{B-G}}$, $\underline{I}_{L_A}$and $\underline{I}_{L_B}$are the involved voltage and current phasors respectively, in this case A and B. The term $R_F\underline{I}_F$is the fault resistance and the current through it and is zero in the classic method. In the other hand, an estimation of the arc resistance is calculated in the RMD method [5]:

$$R_F = \frac{2 \cdot \mathcal{I}m\{(\underline{U}_{L_{A-G}} - \underline{U}_{L_{B-G}}) \cdot [\underline{Z}_L \cdot (\underline{I}_A - \underline{I}_b)]^*\}}{\mathcal{I}m\{2 \cdot j \cdot \sqrt{3} \cdot \underline{I}_2 \cdot [\underline{Z}_L \cdot (\underline{I}_A - \underline{I}_b)]^*\}} \quad \textbf{(2)}$$

Where $\underline{U}_L$ is the measured loop voltage and $\underline{I}_2$ is the negative sequence component of the current. For a phase to ground fault, the ratio between impedance of the earth path and the line impedance is included in the equation. This ratio is a complex number and is called the residual compensation factor which is designated as:

$$\underline{k}_0 = k_r + \mathrm{j} \cdot k_x = \frac{R_G}{R_L} + \mathrm{j} \cdot \frac{X_G}{X_L} \quad \textbf{(3)}$$

The two methods use different equations for determining the Line to ground (L-G) loops. The equation given for the L-G impedance is:

$$\mathrm{R_{L-G}} = \frac{\mathcal{R}e(\underline{U}_{L-G}) \cdot \mathcal{R}e(\underline{I}_L - k_\mathrm{X} \cdot \underline{I}_G) + \mathcal{I}m(\underline{U}_{L-G}) \cdot \mathcal{I}m(\underline{I}_L - k_\mathrm{X} \cdot \underline{I}_G)}{\mathcal{R}e(\underline{I}_L - k_R \cdot \underline{I}_G) \cdot \mathcal{R}e(\underline{I}_L - k_\mathrm{X} \cdot \underline{I}_G) + \mathcal{I}m(\underline{I}_L - k_R \cdot \underline{I}_G) \cdot \mathcal{I}m(\underline{I}_L - k_\mathrm{X} \cdot \underline{I}_G)} \quad \textbf{(4)}$$

$$X_{\mathrm{L-G}} = \frac{\mathcal{I}m(\underline{U}_{L-G}) \cdot \mathcal{R}e(\underline{I}_L - k_\mathrm{X} \cdot \underline{I}_G) - \mathcal{R}e(\underline{U}_{L-G}) \cdot \mathcal{I}m(\underline{I}_L - k_x \cdot \underline{I}_G)}{\mathcal{R}e(\underline{I}_L - k_R \cdot \underline{I}_G) \cdot \mathcal{R}e(\underline{I}_L - k_\mathrm{X} \cdot \underline{I}_G) + Im(\underline{I}_L - k_R \cdot \underline{I}_G) \cdot \mathcal{I}m(\underline{I}_L - k_\mathrm{X} \cdot \underline{I}_G)} \quad \textbf{(5)}$$

$$\underline{Z}_{\mathrm{L-G}} = \mathrm{R_{L-G}} + j \cdot X_{\mathrm{L-G}} \quad \textbf{(6)}$$

Where:

- $\underline{U}_{\mathrm{L-G}}$: Fundamental phase to ground voltage
- φ_U : Angle of the phase to ground voltage
- $\underline{I}_\mathrm{L}$: Fundamental frequency component of the phase current
- $\varphi_{\mathrm{I_L}}$: Angle of the phase current
- $\underline{I}_E$: Fundamental frequency component RMS value of the earth current
- $\varphi_{\mathrm{I_G}}$: Angle of the ground current

The following equation to determine the L-G impedance is the basis of the RMD method:

$$\underline{Z}_{L-G} = \frac{\underline{U}_{L-G} - R_F \cdot \underline{I}_F}{\underline{I}_L - \underline{k}_0 \cdot \underline{I}_G} \quad \textbf{(7)}$$

$\underline{I}_F$ is the fault current which cannot be measured. This can be estimated using the measured negative sequence current ($\underline{I}_2$) or zero sequence current ($\underline{I}_0$). In this document I_0 is used. The following equations are used by RMD where all parameters are set or measured:

$$|\underline{Z}_{L-G}| = \frac{\mathcal{I}m\{\underline{U}_{L-G} \cdot [\underline{I}_0 \cdot e^{j*\delta_{comp}}]\}}{\mathcal{I}m\{\underline{Z}_{LT}\,(\underline{I}_L - \underline{k}_0 \cdot \underline{I}_G) \cdot [\underline{I}_0 \cdot e^{j*\delta_{comp}}]\}} \quad \textbf{(8)}$$

$$X = \frac{\mathcal{I}m\{\underline{U}_{L-G} \cdot [\underline{I}_0 \cdot e^{j*\delta_{comp}}]\}}{\mathcal{I}m\{\underline{Z}_L / |\underline{Z}_{LT}|\,(\underline{I}_L - \underline{k}_0 \cdot \underline{I}_G) \cdot [\underline{I}_0 \cdot e^{j*\delta_{comp}}]\}} \sin\varphi \quad \textbf{(9)}$$

Where $\underline{\boldsymbol{Z}}_{\boldsymbol{LT}}$ is the total impedance of the line. If the impedance angles are not equal, inhomogeneity can be compensated with a parameter using the compensation angles $\boldsymbol{\delta_{comp}}$. This compensation angle compensates for the difference in the R/X ratio between the total network and the fault loop and should be set into the protection relay.

2 Study case

Figure 1 shows the study case in a single line diagram. The grid connects the (wind turbines) WTs to the main transmission grid by a transmission cable. Fault locations and protection relays are also visible in this diagram. The main parts are discussed from left to right.

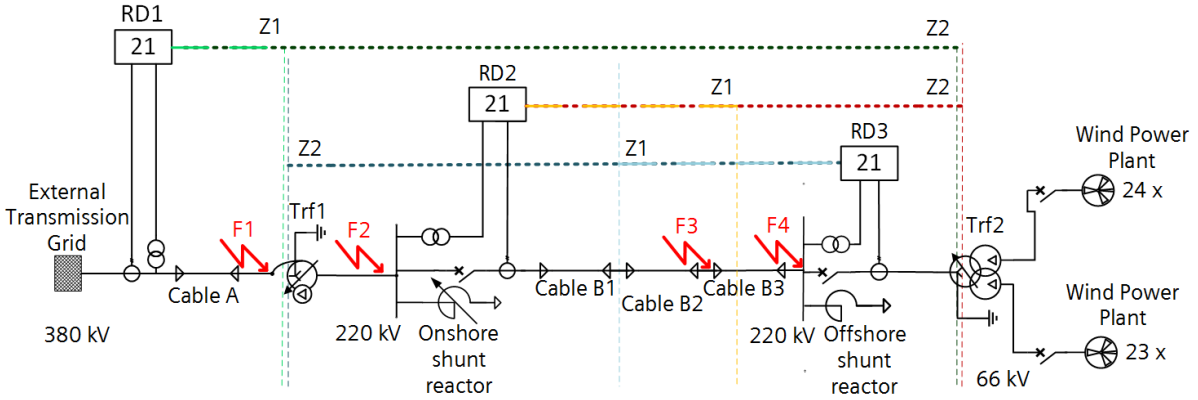

Figure 1: Simplified overview of the wind farm grid as modeled including fault locations.

The wind farm grid is connected to an external 380 kV transmission grid modeled with a weak or strong grid scenario. The autotransformer (trf1) is 380 kV to 220 kV. Cable B is a 60 km long submarine cable divided into three sections (B1, B2, B3). Shunt reactors are placed at both ends of the cable to compensate for the capacitive reactance the cable. Transformer Trf 2 is a three winding transformer connected on the primary side at the 220 kV platform bus. The secondary and tertiary side are both connected to 66 kV wind power plant (WPP) busses. WPP1 has 24 wind turbines evenly divided over three strings. WPP2 has 23 wind turbines divided over three strings. The reactive power setpoint of the wind turbines is set differently for each scenario. Multiple wind turbines (WTs) in a string are modeled together into one aggregated WT model. The distance protection relays (RD1, RD2 and RD3) are located at three locations in the network. The protected areas are denoted with dashed lines. The following grading times are used for the protection relays:

- RD1 Z1: 230 ms Z2: 440 ms
- RD2 Z1: 0 ms Z2: 230 ms
- RD3 Z1: 0 ms Z2: 230 ms

2.1 Description of the fault locations

The fault locations are chosen at the most characteristic locations. The locations of the faults are highlighted in figure 1 and listed below:

- F1: 380 kV terminals of transformer trf1.
- F2: Connection point of cable B to the grid.
- F3: 50 % of the length of cable B.
- F4: 220 kV offshore bus.

Fault locations F1 and F2 are located at an air-insulated substation and thus a potential location for arcing. Therefore, the scenarios with fault locations F1 and F2 are simulated with and without fault resistance. Four simplified arc models with constant resistance and without wind input are applied.
The fault resistances are different for each location and each type of fault. The clearance distance is taken as arc length (l_{arc}). The arc resistance (R_{arc}) is calculated using the following equation [6]:

$$R_{arc} = \frac{E \cdot l_{arc}}{I_{arc}} \quad \textbf{(10)}$$

Where I_{arc} is the fault current and E is a constant of 2500 V/m. The minimum short circuit current is chosen to be the fault current to create the worst-case scenario.

2.2 Wind turbine model

All the components in the network are modeled in a way to recreate the most characteristics behaviors during EMT phenomenon. The WTs use power electronic converters (PEC) and control mechanisms. A Type-3 WT uses a double feed induction (DFIG) machine in which the rotor winding is connected to a PEC (Type-3). While the stator winding is straight connected to a transformer. A correct control of the PEC can set the stator frequency equal to the grid frequency with a varying shaft frequency.
Usually the Type-3 WTs is protected against overloading with a chopper and a crowbar circuit to dissipate excess energy in case of high current flows and protect the PEC.
Multiple standard WT models are considered to be used in the simulation, including WECC [7] and IEC 61400-27-1 [8] based models. The DigSilent® WT library model [9] is chosen because of the compatibility with EMT simulations the possibility to examine and modify the full model.

3 Protection Performance Testing

Several scenarios have been selected to be simulated, with variations in fault location, number of involved phases, arc resistance, grids strength and total amount of power generated in both wind power plants. The process of simulating multiple scenarios is automated with a script. Secondary currents and voltages of the CTs and VTs are extracted from the simulation and saved as Comtrade files. A signal generator can load the Comtrade files and synthesize the signals to be fed into the protection relay. In figure 2 a block diagram of the testing process is shown.
A binary output signal from the signal generator becomes '1' when the comrade file is played. A setting in the protection relay is used as a trigger to record the case. The records from the protection relay are downloaded to the PC and administered in the scenario list. The protection relay settings are computed according to the test grid.

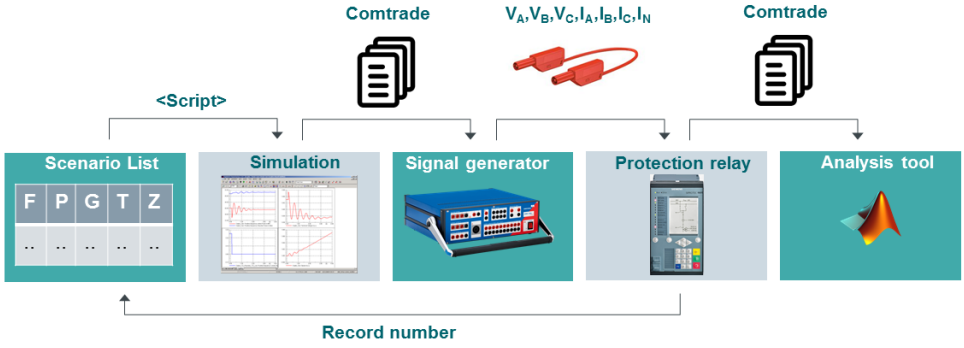

Figure 2: A block diagram of the test setup.

4 Test results and analysis

In this section, the testing methodology is explained and based on this, numerous results are obtained. The tests from this study show that the protection relay does not respond correctly to all scenarios. Tests confirm that the protection relay in 778 of the 874 cases react as expected. The cause of the other 96 cases is unexpected. From all results, special attention is given to the number of maloperations (wrong protection operation) and missed trips (protection fails to eliminate the fault where necessary).
Figure 3 shows a bar graph with the total number of tests and the number of unexpected results for every fault type.
The unexpected results are categorized into groups with similar characteristics such as; fault location, WT infeed and faulty lines. 11% of the cases with the classic method as well as 11% of the cases with the RMD method resulted in an unexpected trip.
However, not all scenarios the unexpected cases using the RMD method are also unexpected using the classic method and vice versa. In the unexpected results of the classic operation 6 % is a missed trip. Using RMD was 8 % a missed trip. The rest of the unexpected results are maloperations.

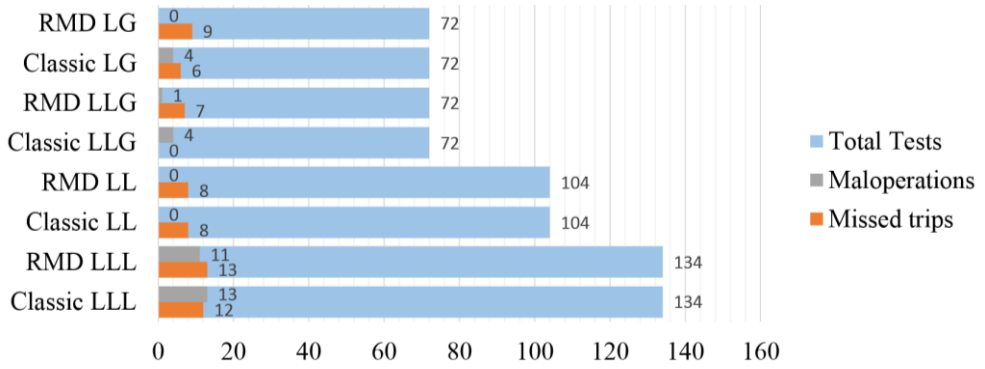

Figure 3: Bar graph with the total number of tests and the number of unexpected results per type of fault.

In the following paragraphs two groups of unexpected results are discussed in detail, which are found to have significant impact on the protection operation.
In the first set of scenarios a 3-phase fault is simulated at the 220 kV terminal of the autotransformer (fault location F2). The result of this test is a maloperation in RD1 and a missed trip in RD2. It is expected that two effects are causing the unexpected results: a radical change of voltage angle after the fault is initiated and a changing fault impedance.
In the second set of scenarios a 2-phase to ground fault is initiated at the 380 kV terminals of the autotransformer (fault location F1). In these scenarios a maloperational trip signal is given while no trip is expected. The impedance is calculated inside zone 2 if the classic method is used. The RMD method does calculate the impedance outside zone 2, no trip was given and does respond as expected.

4.1 Scenario 1: Changing impedance and voltage angle

A 3-phase fault is initiated in the onshore 220 kV bus (fault location F2). The fault resistance is 1.7 Ω. The phenomenon occurs at minimum and maximum grid strength. This result occurs in the cases where the WT are generating at 10%, 70% and 100% of their nominal power. Protection relays RD2 and RD3 do not react as expected. Although RD1 responds as expected. The unexpected result takes place using RMD and the classic method. For one of the set scenarios with this unexpected result RD3 gave a trip signal using RMD while no trip signal was given using the classic method. However, other scenarios still gave an unexpected result using RMD.
Figure 4 shows the impedance trajectory of RD3 (Figure 4a) and RD2 (Figure 4b) for a scenario were the classic method is programed into the protection relays. The designated time points in the plots are briefly described in table 1.

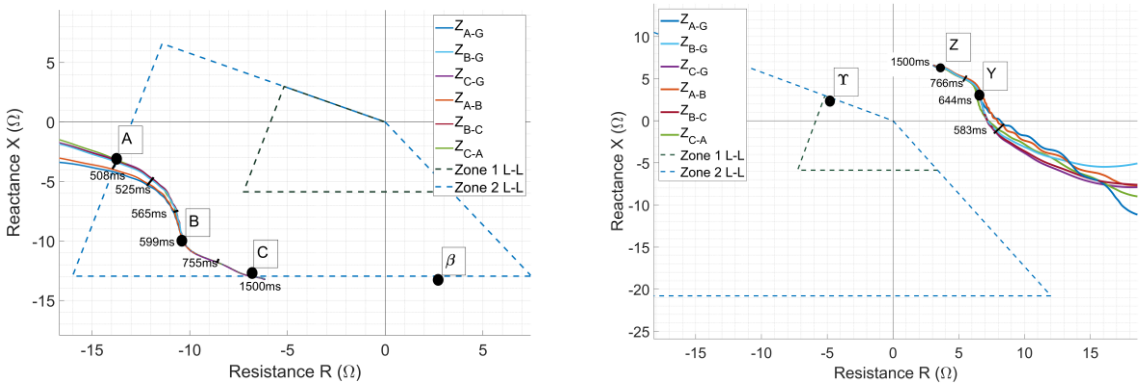

Figure 4: Impedance trajectory of (a) RD3 and (b) RD2

Table 1: Events at multiple times

Designation in figure 4	Time (ms)	Description
A	508	The impedance enters the zone. A pickup is received for the L_{A-G}, L_{B-G}, L_{C-G} fault loops
B	599	The pickup signal is retracted
C	1500	End of the simulated fault
Y	644	A pickup signal is received
Y*	674	A trip signal is received for zone 1
Z	1500	End of the simulated fault

The fault is initiated at 500 ms. Two effects in the grid play a major role. The first is the control of the WT. When the voltage drops, the fault ride through control loop of the WT starts to deliver a higher proportion of reactive power to sustain voltage level within the set boundaries. Seven aggregated WT models activate their crowbar just after the moment that the fault is initiated at 506 ms. The reason is that the rotor current reaches its maximum value. The crowbars are deactivated at 550 ms.
The control of active and reactive power during the fault has a repercussion in the impedance that can be seen in the plots (figure 4). From the results can be calculated that the impedance changes with 34 Ω per second after the transient. In the impedance plot can be seen that the impedance stays in the second zone.
Like any other fault, the fault circuit differs from the normal circuit, the magnitude and angle of impedance immediately change after the fault is introduced. This change in reactance causes the voltage angle measured at the location of the protection relay to rotate. In the simulated scenario the voltage angle does rotate more than 60°.
In RD3 the fault impedance is inside the second zone. Therefore, a trip is expected after the operation delay of 230 ms.
The relay gives a pickup signal when the fault occurs. However, this pickup signal will be turned off after 113 ms and trip command is executed. The fault impedance changes but remains inside the second zone.
RD2 gives a trip signal when no trip is expected. The impedance plot from figure 4b shows that the phase to phase fault impedance is at the opposite site of the zones. However, a trip signal is given by the protection relay. A trip signal is unexpected because the impedance is not inside the zone.
A separate simulation model is adjusted to investigate the influence of the wind turbine control on this scenario. In this simulation, the reactive power control of the wind turbine is interrupted just before the fault is initiated to start the fault in an equal condition. During the fault the control does not have an influence. The impedance stabilizes at a value comparable to the result of an analytical short circuit calculation and manual calculation. A trip signal is initiated in this scenario. This is the expected result and shows that the unexpected behavior is correlated with the wind turbine control.

Expected cause

First will be focused on the behavior of RD3. The protection relay behaves as expected when the fault is initiated. A pick-up signal is received at the moment that the impedance enters the zone. This pick-up signal stays active for 113 ms.
It is assumed that the protection relay switches to another calculation method at the moment that the pick-up falls off. A trigger for the direction determination algorithm to change the calculation method could be the moving impedance. A calculation method using the pre-fault voltage rotates the impedance outside the zone. The pre-fault voltage has another angle (φ_U). The result of the new calculation sets the impedance outside the zone. If the protection relay concludes that the impedance is outside the zone it does retract the pick-up signal.
Essentially the same occurs at RD2. However, the second calculation method sets the impedance inside the zone. The calculated loop impedance with the pre-fault voltage is designated in figure 4b with ϒ for RD2 and β for RD3.

Switching to another calculation method is normal for a numerical distance protection relay. Multiple calculation methods are used depending on the time and depth of impedance into a zone. Hermann [10] gives a detailed description about this process in his book. In a separate test where the signal is stabilized after 520 ms shows that this switching of calculation method is induced by the moving impedance. This assumption could not be punctually corroborated because more information is needed on the internal working of the protection relay.

4.2 Scenario 2: Arc-resistance reduces calculated impedance

This phenomenon does only take place with RD3 and only with the classic distance protection method. This is the only protection relay which protects in the direction of the external grid. Every scenario has an LLG fault at location F1 and a fault resistance of 2.25 **Ω**. The generated power from the WT is 10%. The unexpected result does only occur at minimum grid strength for the LLG fault. It has been observed that at maximum grid strength the L-G loop impedance has also an incorrect value. Most of the current flows through the fault resistance to ground.

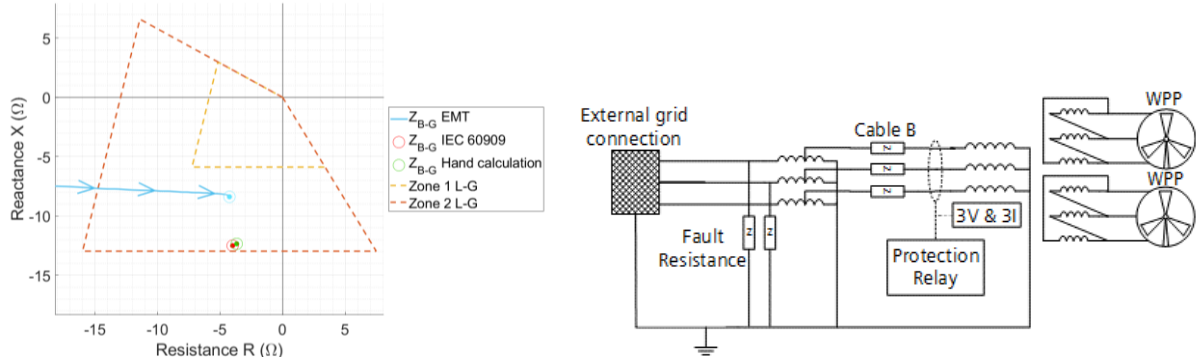

(a) **(b)**

Figure 5: Impedance plot the L-G fault loop impedance measured with RD3.

The fault at location F1 is outside the area protected by RD3. Nevertheless, the impedance is calculated inside zone 2. Figure 5 shows the impedance plot of this scenario with multiple calculation methods. For this scenario no test is needed because of the steady state. The extraction from the simulation could be imported directly into the analysis tool to see the impedance plot. Therefore, this unexpected result is not caused by the protection relay.

Expected cause

A calculation is carried out manual to give a deep insight into what happens in the grid. The sequence networks method is used [11].
The voltage drop over the fault impedance is not included in the classic method while RMD is specially designed to estimate the arc resistance [12]. This is the main cause of the unexpected behavior of this scenario. The fault is close to the external grid. Therefore, the current contribution from the grid is relatively high and causes a high voltage drop over the fault impedance. The relay cannot detect this high current since it is located at the WPP side fault.
The voltage over the fault impedance is calculated. The fault voltage in the L_{B-G} loop has a magnitude of 15 kV. This is significant since the voltage measured by RD3 has a magnitude of 52 kV.
The phenomenon that an increase of fault impedance decreases the measured impedance is explained by the significant voltage drop over the fault impedance. Most of the current through the fault impedance is supplied by the external grid. A higher fault impedance means a higher voltage drop over the fault impedance. This results in a calculated impedance value which differs from the real

5 Discussion

In this paper, the performance of the distance protection relay in an offshore transmission grid is analyzed. The relay is tested over a wide range of situations, including multiple infeed levels from the wind power plant.

5.1 Performance of the classic distance protection and distance protection with reactance method.

The classic distance protection and the RMD method perform similarly, focusing on the percentage of unexpected results. However, the number of maloperations is 8 % using the classic method, and only 3 % using the RMD method. Maloperations could be classified as a more severe concern than missed trips since a fault could be detected and isolated by another protection relay. However, a maloperation can isolate a part of the grid in normal conditions.

5.2 Large fault resistance

Other studies have found that the fault is not always detected if the fault resistance is too large. [2]. Section 2.1 describes the determination of the fault resistance, which is 2.25 Ω at maximum. No scenario is found where the fault impedance exceeds the R-reach of the zone. However, in scenario 2 does the fault impedance cause a decrease of the calculated L-G loop impedance. In these cases, a trip signal is sent, while no trip signal is expected.

The L-G loop impedance calculation with the classical method does not account for the relatively high voltage drop over the fault resistance. The main contributor of the current through the fault resistance is from the external grid. This is a remote end component that is not measured by the protection relay which increases the deviation on the calculated fault impedance with the classic method [13] [14]. The RMD method takes the fault resistance into account and acts therefore as expected.

5.3 Low energy production

Multiple studies report on unreliable behavior of distance protection if generation is low [2] [3]. Many tests from this study confirm this statement. It is expected that the influence of maloperation by the distance protection at low generation is low in most cases. This is not a problem since the other protection functions and other relays will take over and open the CB.

5.4 Crowbar

During the analysis, special attention is put the crowbar effect. Caution has been taken due to crowbar operation as mentioned by Lina He and Liu [15]. The crowbar circuit affects the impedance measurement by the distance protection relay. In the WT model the crowbar is activated in some scenarios. However, no scenario where the crowbar circuit causes an unexpected result is found. This could be explained since a transformer is located between the measurement point at RD3 and the WT. The impedance of this transformer will be enough to set the measured impedance outside the protected zone.

CONCLUSION

Several fault scenarios have been simulated in a wind farm grid model in this study. The scenarios had different kinds of faults on different locations. The signals from the CTs and VTs are extracted and synthesized fed to a protection relay. Finally, the response of the protection relay is analyzed.

Overall, the relay behaves according to the expectation. Nevertheless, two unexpected result scenarios were distinguished, catalogued, and analyzed in detail in this work. A changing impedance, voltage angle jump and large fault impedances can make the distance protection less reliable.

The percentage of unexpected results between the classic method and the RMD method are comparable. However, the maloperations percentage using the RMD method is lower than the percentage using the classic method.

This paper gives inside in the behavior of both distance protection methods in equal fault conditions. Distance protection is an effective protection function. However, every protection function has its limitation. This study can help with the development of a suitable a protection philosophy. For maximum protection it is recommended to use multiple protection functions in parallel. The selected distance protection method(s) must be fitted to the specific power system to be protected.

BIBLIOGRAPHY

[1] European Commission, “2030 climate & energy framework,” September 2020.

[2] S. De Rijcke, C. Moors, P. Souto Perez et J. Driesen, “Impact of wind turbines equipped with doubly-fed induction generators on distance relaying,” *in IEEE PES General Meeting*, 2010.

[3] G. Li, B. Zhang, J. Wang, Z. Hao, Z. Bo et D. Writer, “Wind Farm Electromagnetic Dynamic Model and Outgoing Line Protection Relay RTDS Testing,” *in VDE, Soest*, Germany, 2011.

[4] J. Chavez, M. Popov, R. Dubey, et al, “Exposing available distance relay operations near high wind penetration,” *in Protection, Automation & Control World (pacworld) Conference*, Sofía, Bulgaria, 2018.

[5] Siemens AG, “Manual Distance and Line Differential Protection, Breaker Management for 1-Pole and 3-Pole Tripping 7SA87, 7SD87, 7SL87, 7VK87,” 07 2018.

[6] G. Ziegler, “Distance Protection for transformers,” in “Numerical Distance Protection”, Erlangen, Germany, Publics Corporate Publishing, 2011, pp. 167-180.

[7] M. Walter, “Der Selektivschutz nach dem Widerstandsprinzip,” Techn. Hochschule Aachen, Aachen, 1932.

[8] P. Pourbeik, “WECC Second Generation Wind Turbine Models,” Electric Power Research Institute, 2014.

[9] H. Hermann, “digitale schutztechnik,” VDE-Verlag GmbH, 1997.

[10] DIgSILENT GmbH, “Template Documentation DFIG Template,” DIgSILENT, 2017.

[11] L. He and C.-C. Liu, “Impact of LVRT capability of wind turbines on distance protection of ac grids,” in Innovative Smart Grid Technologies (ISGT), 2013 IEEE PES. IEEE, 2013, pp. 1–6.

[12] J. J. Grainger, W. D. Stevenson et G. W. Chang, Power system analysis, Mcgraw-Hill Education - Europe, 2003.

[13] C. Dzienis, Y. Yelgin, G. Steynberg et M. Claus, “Novel impedance determination method for phase-to-phase loops,” in Power Systems Computation Conference, Wroclaw, Poland, 2014.

[14] M. Washer, J.-C. Maun, C. Dzienis, M. Kereit, Y. Yelgin et J. Blumschein, “Precise impedance based fault location algorithm with fault resistance separation,” in IEEE Eindhoven PowerTech, Eindhoven, Netherlands, 2015.

[15] C. Dzienis, Y. Yelgin, M. Washer et J.-C. Maun, “Accurate impedance based fault location algorithm using communication between protective relays,” in Modern Electric Power Systems (MEPS), Wroclaw, Poland, 2015.

[16] L. He, C.C. Liu, “Impact of LVRT capability of wind turbines on distance protection of AC grids,” Innovative Smart Grid Technologies (ISGT), 2013 IEEE PES, pp. 1-6, 2013.